

Deep Markov Spatio-Temporal Factorization

Amirreza Farnoosh¹, Behnaz Rezaei¹, Eli Zachary Sennesh², Zulqarnain Khan¹, Jennifer Dy¹, Ajay Satpute³, J Benjamin Hutchinson⁴, Jan-Willem van de Meent¹, Sarah Ostadabbas¹

¹ Department of Electrical and Computer Engineering, Northeastern University, Boston, Massachusetts, USA.

² Khoury College of Computer Science, Northeastern University, Boston, Massachusetts, USA.

³ Department of Psychology, Northeastern University, Boston, Massachusetts, USA.

⁴ Department of Psychology, University of Oregon, Eugene, Oregon, USA.

Abstract. We introduce deep Markov spatio-temporal factorization (DMSTF), a deep generative model for spatio-temporal data. Like other factor analysis methods, DMSTF approximates high-dimensional data by a product between time-dependent weights and spatially dependent factors. These weights and factors are in turn represented in terms of lower-dimensional latent variables that we infer using stochastic variational inference. The innovation in DMSTF is that we parameterize weights in terms of a deep Markovian prior, which is able to characterize nonlinear temporal dynamics. We parameterize the corresponding variational distribution using a bidirectional recurrent network. This results in a flexible family of hierarchical deep generative factor analysis models that can be extended to perform time series clustering, or perform factor analysis in the presence of a control signal. Our experiments, which consider simulated data, fMRI data, and traffic data, demonstrate that DMSTF outperforms related methods in terms of reconstruction accuracy and can perform forecasting in a variety domains with nonlinear temporal transitions.

Keywords: Deep learning, Factor analysis, fMRI, Markov process, Variational inference.

1 Introduction

Analysis of large-scale spatio-temporal data is relevant to a wide range of applications in biology, marketing, traffic control, climatology, and neuroscience. Due to the high dimensionality of the data, methods for spatiotemporal analysis either exploit smoothness and correlations in the signal [4,26], or map high-dimensional data onto a lower-dimensional representation [37,44,39,2,6,45,8].

In this paper, we combine these two principles by building on recent approaches for hierarchical probabilistic factor analysis [25,24,35]. These models represent data $Y \in \mathbb{R}^{T \times D}$ with T temporal and D spatial dimensions as a product $Y \simeq W^\top F$ between temporal weights $W \in \mathbb{R}^{T \times K}$ and spatial factors

$F \in \mathbb{R}^{K \times D}$. Hierarchical approaches to probabilistic factor analysis explicitly model the correlations between multiple instances $\{Y_1, \dots, Y_N\}$ by representing W_n and F_n in terms of some set of latent variables Z_n that are drawn from a shared prior. The result is a modeling framework that performs two levels of dimensionality reduction. At the instance level, the model represents high-dimensional spatio-temporal data Y_n in terms of lower-dimensional matrices W_n and F_n . At the level of the corpus, we further reduce dimensionality by learning a mapping from latent variables Z_n to weights and factors.

The main contribution of this paper is that we develop methods for hierarchical probabilistic factor analysis that uncover common patterns of temporal variation across instances and are amenable to temporal forecasting. To this end, we introduce deep Markov spatio-temporal factorization (DMSTF), a model that learns a deep generative Markovian prior in order to reason about (potentially nonlinear) temporal dynamics forecasting.

DMSTF is related to recent studies that employ temporal smoothness assumptions [9] or more explicitly model dynamics [37,44,39,33,17,2,6] for matrix factorization of multidimensional times series. While most of these methods are not essentially probabilistic (providing only point estimates for imputation/prediction tasks), some Bayesian probabilistic matrix factorization methods have been proposed [34,45,8], and linear temporal dynamics on factor latents, W_n , have been adapted to these methods in [43,7,38]. However, these methods do not explicitly adopt *a priori* assumptions about functional form of spatial factors, F_n , when available. This makes them intractable for extremely high dimensional spatial data such as neuroimaging data. Moreover, the linear dynamical assumptions in these methods fall short of modeling potentially nonlinear transitions.

DMSTF builds on topographic factor analysis (TFA) [25] and neural topographic factor analysis (NTFA) [35], which were designed with neuroimaging applications in mind. However, the DMSTF generalizes from both these models, specifically by modeling temporal dynamics, hence, can be applied to spatio-temporal analysis more generally. We demonstrate this in our experiments, which evaluate model performance on simulated data, two large-scale fMRI datasets, and four traffic datasets. Our experiments demonstrate that DMSTF achieves better predictive performance for unseen data relative to existing baselines, both when evaluating the log-likelihood for new instances and when performing next time-point forecasting.

We summarize the contributions of this paper as follows:

- DMSTF learns a deep Markovian prior that represents high-dimensional spatio-temporal data in terms of low-dimensional latent variables that can capture nonlinear dynamics of the data.
- DMSTF learns a mapping from latent variables to spatial factors and temporal weights, which provide an intermediate representation for downstream regression or classification tasks.
- DMSTF is able to perform clustering in the low-dimensional temporal latent space, which can provide visual insights about data.

- DMSTF introduces a control input that can be used for semi- or fully-supervised factorization.

The remainder of this paper is structured as follows. Section 2 presents an overview of related work. Section 3 described the DMSTF model architecture. Section 4 provides details on model training. Section 5 describes experiments on simulated data, neuroimaging datasets and traffic datasets.

2 Related Works

Factor analysis has been extensively used for reducing dimensionality in spatio-temporal data. Principal component analysis (PCA) [29] and independent component analysis (ICA) [11] are among the most well-known classical factor analysis methods. To accommodate tensor data, and mitigate scalability issues, multilinear versions have been proposed [15,32,10,41]. These methods do not naturally handle missing data. They are also permutation invariant along the batch dimension, and therefore cannot capture temporal dynamics [44]. Spatial factors obtained by these methods are also unstructured and difficult to interpret in many applications. In an early attempt to get temporally smooth structures, Chen and Cichocki [9] developed a non-negative matrix factorization model and applied temporal smoothness and spatial decorrelation regularizers to achieve physiologically meaningful components.

Since then, several matrix/tensor factorization approaches have been proposed for modeling temporal dynamics in multivariate/multidimensional time series. Sun et al. [37] presented a dynamic matrix factorization suited for collaborative filtering setting in recommendation systems using a linear-Gaussian dynamical state space model. Yu et al. [44] proposed to use an autoregressive temporal regularizer for matrix factorization to describe temporal dependencies in multivariate time series. [39] added an additional graph Laplacian regularizer to learn spatial autocorrelations and perform prediction on unknown locations. [33] applied multilinear dynamical systems to the latent core tensor obtained from Tucker decomposition of tensor time series data, similarly to [17]. Bahador et al. [2] enforced a low rank assumption on coefficient tensor of vector autoregressive models, and used a spatial Laplacian regularization for prediction in spatio-temporal data. [6] developed a probabilistic temporal tensor decomposition that models temporal dynamics in latent factor using a multilinear Gaussian distribution with a multilinear transition tensor (using multilinear dynamical system) with additional contextual constraints.

In contrast to the the methods above, which provide point estimates for imputation/prediction tasks, Bayesian probabilistic matrix/tensor factorization methods have been proposed (see [34,45,8]). In these approaches, latent factors have Gaussian priors, and Markov chain Monte Carlo (MCMC) methods are used for approximate inference in training and imputation. However, these models essentially focus on global matrix/tensor factorization without explicitly modeling the local temporal and spatial dependencies between factors. Hence, linear temporal dynamics on factor latents have been adapted to Bayesian Gaussian tensor

factorization in [43,7,38]. While some of these methods have been effective in dynamical modeling of multidimensional time series, they do not explicitly adopt any functional form for the spatial domain, which makes them less effective for high dimensional spatial data such as fMRI. Moreover, the linear dynamical assumptions in these methods lack the capacity to characterize complex nonlinear dependencies.

Motivated by recent advances in deep learning, several papers have studied incorporation of neural networks into Gaussian state space models for nonlinear state space modelling [21,42,22,13,18,3]. A common practice is to learn a low-dimensional temporal generative model with an encoding scheme for performing amortized inference. However, these models are not applicable to high dimensional spatio-temporal data without factorization assumptions, and are not tractable in the case of missing data.

A number of fMRI-specific generative models have been proposed in which spatial factors are parameterized by Gaussian kernels to enhance interpretability [24,25,35]. The most closely related of these is NTFA [35], which represents the neuroimaging data for each trial, Y_n , in terms of an embedding for the participant, $Z_{p(n)}$, and an embedding for the stimulus, $Z_{s(n)}$, which allows the model to capture commonalities in trials associated with a particular participant and stimulus. However, NTFA and other TFA variants assume a prior in which weights are conditionally independent as a function of time, which means that these models do not explicitly encode temporal dynamics. In this sense, DMSTF, which does reason about temporal dynamics, but does not explicitly model the interaction between participants and stimuli, is complementary to NTFA.

3 Deep Markov Spatio-Temporal Factorization

Model Structure and Variational Inference: DMSTF defines a hierarchical deep generative model for a corpus of instances $\{Y_1, \dots, Y_N\}$,

$$\begin{aligned} Y_n &\sim \text{Norm}(W_n^\top F_n, \sigma^Y I), \\ W_n &\sim \text{Norm}(\mu_\theta^W(Z_n), \sigma_\theta^W(Z_n)), \\ F_n &= \Phi(H_n), & H_n &\sim \text{Norm}(\mu_\theta^F(Z_n), \sigma_\theta^F(Z_n)), \\ Z_n &\sim p_\theta(Z). \end{aligned}$$

Here $p_\theta(Z)$ is a deep generative prior over a low-dimensional set of local (instance-level) variables Z_n . The temporal weights W_n are sampled from a Gaussian distribution that is parameterized by neural networks μ_θ^W and σ_θ^W . The spatial factors are defined as a deterministic transformation $\Phi(H_n)$ of a set of factor parameters H_n , which are sampled from a distribution that is parameterized by neural networks μ_θ^F and σ_θ^F . All networks have parameters, which we collectively denote by θ .

We train this model using stochastic variational methods [14,30,20,31]. These methods approximate the posterior $p_\theta(W, H, Z | Y)$ using a variational distribu-

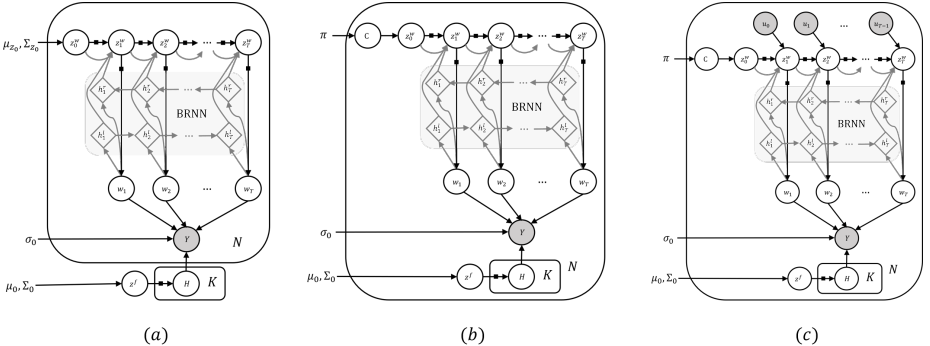


Fig. 1. Graphical model for three variants of DMSTF. Gray lines represent variational distribution.

tion $q_\phi(W, H, Z)$ by maximizing a lower bound $\mathcal{L}(\theta, \phi) \leq \log p_\theta(Y)$

$$\begin{aligned}\mathcal{L}(\theta, \phi) &= \mathbb{E}_{q_\phi(W, H, Z)} \left[\log \frac{p_\theta(Y, W, H, Z)}{q_\phi(W, H, Z)} \right] \\ &= \log p_\theta(Y) - \text{KL}(q_\phi(W, H, Z) \parallel p_\theta(W, H, Z \mid Y)).\end{aligned}$$

By maximizing this bound with respect to the parameters θ , we learn a deep generative model that defines a distribution over datasets $p_\theta(Y)$, which captures correlations between multiple instances Y_n of the training data. By maximizing the bound with respect to the parameters ϕ , we perform Bayesian inference by approximating the distribution $q_\phi(W, H, Z) \simeq p_\theta(W, H, Z \mid Y)$ over latent variables for each instance.

Model Variants: We will develop three variants of DMSTF, which differ in the set of latent variables Z that they employ. The graphical models for these model variants are shown in Fig. 1. All three models incorporate a deep generative Markovian prior to represent temporal variation in W . To do so, they introduce a set of time-dependent weight embeddings z_t^w to define the distribution on each row w_t of the weight matrix W . Moreover, the K rows of the factor matrix are sampled from a shared prior, which is conditioned on a factor embedding z^f . The models differ in the following ways:

- **Fig. 1(a)**: This model simplifies the structure described above by assuming that the factor parameters H_n and embeddings z_n^f do not vary across instances, but are instead shared at the corpus-level.
 - **Fig. 1(b)**: This model introduces an additional discrete assignment variable c for each instance, which serves to perform clustering on time series.
 - **Fig. 1(c)**: This model additionally introduces a sequence of observed control variables $\{u_0, \dots, u_{T-1}\}$ that condition the distribution $p_\theta(z_t | z_{t-1}, u_{t-1})$.

Derivation of the evidence lower bound for variant (c) of DMSTF is detailed in Appendix A.

Markovian Temporal Latent: We assume a Gaussian distribution for the latent transition probability. Given the latent z_{t-1}^w we parameterize the mean and covariance of the diagonal Gaussian distribution $p_\theta(z_t^w | z_{t-1}^w)$ using a neural network. In the model in Fig. 1(c) this distribution $p_\theta(z_t^w | z_{t-1}^w, u_{t-1})$ is additionally conditioned on a control variable u_{t-1} . Concretely, we pass z_{t-1}^w (and u_{t-1} when applicable) to a multilayer perceptron (MLP) for estimating the Gaussian parameters. We combine a linear transformation of z_{t-1}^w with the estimated mean from the neural network to support both linear and nonlinear dynamics [22]:

$$\mu_{z_t^w} = (1 - g) \odot \mathbb{L}_\theta(z_{t-1}^w) + g \odot \mathbb{F}_\theta(z_{t-1}^w, u_{t-1}),$$

where $\mathbb{L}_\theta(\cdot)$ is a linear mapping, $\mathbb{F}_\theta(\cdot)$ is the nonlinear mapping of neural network, and $g \in [0, 1]$ is a scaling vector which itself is estimated from z_{t-1}^w using a neural network. We show the neural network architectures we employ in Table 1.

Clustering Latent: In the models in Fig. 1(b) and Fig. 1(c), we assume that each sequence Y_n belongs to a specific state out of S possible states, and is determined by the categorical variable c_n in our temporal generative model. This is sampled from a categorical distribution $c_n \sim \text{Cat}(\pi)$, where $\pi = [\pi_1, \dots, \pi_S]$ specifies cluster assignment probabilities. To this end, we assume that the first temporal latent $z_{n,0}^w$ is distributed according to a Gaussian mixture:

$$p_\theta(z_{n,0}^w | c_n = s) = \text{Norm}(\mu_s, \Sigma_s),$$

where the cluster assignment c_n enforces μ_s and diagonal covariance Σ_s .

Temporal & Spatial Factors: As with the transition model, we assume Gaussian distributions for temporal weights, and spatial factors. We parameterize the diagonal Gaussian distributions for temporal weights $p_\theta(w_t | z_t^w)$ and factor parameters $p_\theta(H | z^f)$ with neural networks. z^f itself is sampled from a normal distribution: $z^f \sim \mathcal{N}(0, I)$. Introducing z^f as a low dimensional spatial embedding in the model encourages estimation of a multi-modal distribution among spatial factors.

The form of the spatial factor parameters H depends on the task at hand. In the case of fMRI data, we employ the construction used in TFA [25,24,35], which represents each factor as a radial basis function with parameters $H_k = \{\rho_k, \gamma_k\}$:

$$F_{kd}(\rho_k, \gamma_k) = \exp \left(- \frac{\|\rho_k - r_d\|^2}{\exp(\gamma_k)} \right), \quad (1)$$

This parameterization represents each factor as a Gaussian “blob”. The vector $r_d \in \mathbb{R}^3$ denotes the position of voxel with index d . The parameter $\rho_k \in \mathbb{R}^3$ denotes the center of the Gaussian kernel, whereas $\gamma_k \in \mathbb{R}$ controls its width. In the case of traffic forecasting experiments, we learned spatial factors without any functional form constraints, hence, H directly parameterized $\{F_{kd}\}_{k=1, d=1}^{K, D}$ by mean and covariance of a Gaussian distribution (i.e., $\Phi(\cdot)$ is basically an identity mapping here).

Table 1. Network architecture.

$p_{\theta}(z_t^w [z^w, u]_{t-1})$	$p_{\theta}(w_t z_t^w)$	$p_{\theta}(H z^f)$	$q(z_t^w z_{t-1}^w, w_{1:T})$
$[z^w, u]_{t-1}$ (1) $\in \mathbb{R}^{D_z, D_u}$	$z_t^w \in \mathbb{R}^{D_z}$	$z^f \in \mathbb{R}^{D_z}$	z_{t-1}^w (1), $h_t \in \mathbb{R}^{D_z, 2D_t}$
FC $(D_z + D_u) \times D_t$ ReLU FC $D_t \times D_z$ Sigmoid $g \in \mathbb{R}^{D_z}$	FC $D_z \times D_e$ ReLU FC $D_e \times 2D_e$ ReLU FC $2D_e \times 2K$	FC $D_z \times 2D_z$ ReLU FC $2D_z \times 4D_z$ ReLU (1) FC $4D_z \times 6K$	$\frac{(1)}{2} FC D_z \times 2D_t$ $\frac{h_t + (2)}{2} FC 2D_t \times D_z$ $\mu_{z_t^w} \in \mathbb{R}^{D_z}$ $\frac{h_t + (2)}{2} FC 2D_t \times D_z$ $\log \sigma_{z_t^w} \in \mathbb{R}^{D_z}$
(1) FC $(D_z + D_u) \times D_t$ ReLU FC $D_t \times D_z$ $\mu_{z_t^w}$ Nonlinear $\in \mathbb{R}^{D_z}$ (1) $\tilde{FC} (D_z + D_u) \times D_z$ $\mu_{z_t^w}$ Linear $\in \mathbb{R}^{D_z}$ (2) ReLU FC $D_z \times D_z$ $\log \sigma_{z_t^w} \in \mathbb{R}^{D_z}$	$(\mu, \log \sigma)_{wt} \in \mathbb{R}^{K, K}$	$\mu_{\rho, \gamma} \in \mathbb{R}^{3K, 3K}$ (1) FC $4D_z \times K$ $\log \sigma_{\rho} \in \mathbb{R}^K$ (2) ReLU FC $K \times 1$ $\log \sigma_{\gamma} \in \mathbb{R}$	ALT. (1) FC $4D_z \times 2KD$ $(\mu, \log \sigma)_H \in \mathbb{R}^{KD, KD}$

Variational Distribution: We introduce trainable variational parameters (mean and sigma of a diagonal Gaussian) for each data point in our dataset to define a fully-factorized (i.e. mean-field) variational distributions on the variables

$$\left\{ q(z_{n,0}^w; \lambda_{n,0}^w), q(w_{n,t}; \lambda_{n,t}^w), q(z_n^f; \lambda_n^f), q(H_n; \lambda_n^H) \right\}_{n=1, t=0}^{N, T}$$

We use a structured variational distribution for the variables $q_{\phi}(z_{1:T}^w | w_{1:T})$ in the form of a one-layer bidirectional recurrent neural network (BRNN) with ReLU activation, which is then combined with z_{t-1}^w through another neural network to form distribution parameters of z_t^w :

$$z_t^w \sim \mathcal{N}(\mu_t^w, \Sigma_t^w), \quad \{\mu_t^w, \Sigma_t^w\} = f_{\phi}(z_{t-1}^w, h_t), \quad h_{1:t} = \text{BRNN}_{\phi}(w_{1:T}).$$

where f_{ϕ} is a nonlinear mapping parameterized by an MLP, and Σ is diagonal.

Although we can define variational parameters for categorical distributions $q(c_n)$, we approximate it with posterior $p(c_n | z_{n,0}^w)$, as suggested in [16], to compensate information loss induced by the mean-field approximation:

$$q(c_n) \simeq p(c_n | z_{n,0}^w) = \frac{p(c_n)p(z_{n,0}^w | c_n)}{\sum_{s=1}^S p(c_n = s)p(z_{n,0}^w | c_n = s)}.$$

Kullback Leibler Divergence Terms: A significant advantage of our formulation is that we can analytically calculate the KL terms of evidence lower bound for both multivariate Gaussian, and categorical distributions, which leads to lower variance gradient estimates, and faster training as compared to e.g., noisy Monte Carlo estimates often used in literature.

4 Training Details

We describe the network architectures for the neural networks used in DMSTF in Table 1, where D_z is the dimension of z^w and z^f , and D_t and D_e are the

dimensions of hidden layers for Markovian and temporal latents respectively. For all the experiments in this paper, we assume $D_z = 2$ (except for traffic dataset). We did all the programming in PyTorch v1.3 [28], and used the Adam optimizer [19] with learning rate of 1×10^{-2} . We initialized all the parameters randomly except for spatial locations of fMRI data which we set the initial values to the local extrema in their averaged fMRI data. We clipped spatial locations and scales to the confines of the brain if needed. We used KL annealing [5] to suppress KL divergence terms in early stages of training, since these terms could be quite strong in the beginning, and we do not want them to dominate the log likelihood term (which controls reconstruction) in early stages. We used a linear annealing schedule to increase from 0.01 to 1 over the course of 100 epochs. The number of learnable parameters in our model is dominated by w_t parameters, and therefore will be $O(KNT)$. We run and learn all of the models on an Intel Core i7 CPU @3.7 GHz with 8 Gigabytes of RAM, which proves tractability of the learning process. Per-epoch training time varied from 0.1 in small datasets to 6.0 minutes in larger experiments.

Test/Prediction: We evaluate the performance of DMSTF for short-time prediction tasks (one-point-ahead forecasting) by adopting a rolling prediction scheme as in [8,44]. We predict observations for the next time point using the generative model and spatial factors: $\hat{Y}_{t+1} = \hat{w}_{t+1}^\top F$, where $\hat{w}_{t+1} \sim p(\hat{w}_{t+1} | \hat{z}_{t+1})$, and $\hat{z}_{t+1} \sim p(\hat{z}_{t+1} | z_t)$. Then, we fix the parameters of the generative model and variational parameters for spatial factors, and update variational parameters for z_{t+1}, w_{t+1} using Y_{t+1} , the actual observation at $t + 1$ (running model for a few epochs). We repeat these steps to make predictions in a rolling manner across a test dataset.

5 Experimental Results

5.1 Toy Example

We generated $N = 100$ synthetic spatio-temporal data with $T = 15, K = 2$ using a nonlinear dynamical model (motivated by [22]):

$$z_t \sim \mathcal{N}\left(\begin{bmatrix} \rho z_{t-1}^0 + \tanh(\alpha z_{t-1}^1) & \rho z_{t-1}^1 + \sin(\beta z_{t-1}^0) \end{bmatrix}, 1\right), w_t \sim \mathcal{N}(0.5z_t, 0.1)$$

where $\rho = 0.2, \alpha = 0.5, \beta = -0.1$. For spatial factors, F , we picked two Gaussian blobs centered at $\pm(7.5, 7.5, 7.5)$ with scales of 3, 4.5 respectively in a box of $30 \times 30 \times 30$ at origin. And finally generated $\{Y_n = W_n^\top F\}_{n=1}^N$ with additive noise. We train DMSTF with this synthetic dataset, and estimate the parameters of the model given the functional forms of the generative model. As depicted in Fig. 2 (a) DMSTF is able to recover the actual values of the parameters.

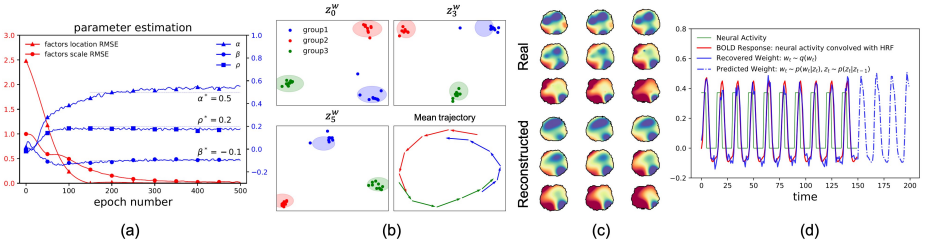


Fig. 2. (a): DMSTF recovers the actual parameters of a nonlinear dynamical system in our toy example. (b): DMSTF recovered the three clusters of activation in our synthetic fMRI dataset, unsupervised. (c): Real and reconstructed brain images. (d): The learned generative model’s predictions show that DMSTF captured the nonlinear hemodynamic response function.

5.2 Synthetic Data

We generate synthetic fMRI data using a MATLAB package provided by [25], which is known to be useful for analysing fMRI models. The synthesized brain image for each trial (time point) is a weighted summation of a number of radial basis functions (spatial factors) randomly located in the brain. The synthesized fMRI data is then convolved with a Hemodynamic Response Function (HRF), and finally we add zero-mean Gaussian noise with a medium-level signal-to-noise ratio. Here, we considered 30 activation sources (spatial factors) randomly located in a standard MNI-152-3mm brain template with roughly 270,000 voxels, and 150 trials. We randomly split these 30 activation sources into 3 groups, each having 10 of the Gaussian blobs. These three groups of sources are periodically activated in turn (according to some random weights) for 5 trials. We generated non-overlapping sequences of $T = 5$ time points from this synthetic fMRI data. This resulted in 10 data points for each activation group ($N = 30$). In order to train DMSTF, we set $T = 5$, $K = 30$, $D_t = 2$, $D_e = 8$, $S = 3$, and $\sigma_0 = 1 \times 10^{-2}$. As depicted in Fig. 2 (b), our model was able to successfully recover the 3 clusters of activation that were present in the dataset in a totally unsupervised manner. Predictions of learned generative model are visualized in Fig. 2 (d), which proves that we were able to capture nonlinear hemodynamic response function by using multi-layer perceptrons in our temporal generative model.

5.3 Neuroimaging Datasets

Autism Dataset: We used the publicly available preprocessed resting state fMRI (rs-fMRI) data from the Autism Brain Imaging Data Exchange (ABIDE) collected at 16 international imaging sites [12]. This dataset includes rs-fMRI imaging from 408 individuals suffering from Autism Spectrum Disorder (ASD), and 476 typical controls. Each scan has $T = 145 \sim 315$ time points at $TR = 2$, and $D = 271,633$ voxels. We split the signals into sequences of 75 time

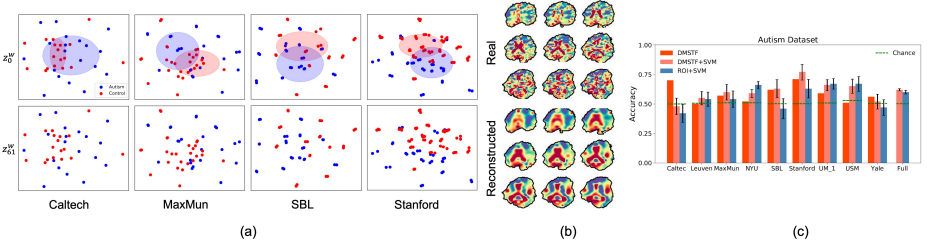


Fig. 3. (a): DMSTF’s clustering results show that the ASD and control groups can be partially separated. (b): Real and reconstructed brain images, showing the smoothing given by sparse factorization. (c): A downstream classification task showed that DMSTF and DMSTF+SVM outperformed regions of interest (ROI)+SVM in the Caltech, MaxMun, SBL, Stanford, and Yale subsets of the data. ROI+SVM performed better in the NYU subset.

points. We take two approaches to evaluate the performance of our model in separating ASD from control: (1) Cluster data directly in the low dimensional latent, z^w , using the clustering feature of DMSTF (called DMSTF), (2) Extract functional connectivity matrices from learned weights, W , followed by a 10-fold SVM for classification (called DMSTF+SVM). As a baseline, we performed a 10-fold SVM classification on extracted connectivity matrices from averaged signals of 116 regions of interest (ROIs) in AAL atlas [40] (called ROI+SVM). Several studies have been done on this dataset to differentiate ASD group from control, all of them using supervised methods, and could achieve accuracies up to 69% (by carefully splitting data to be as homogeneous as possible, and reducing site-related variability) using the signals extracted from anatomically labeled regions in the brain [1,27,36]. We set $T = 75$, $K = 100$, $D_e = 15$, $D_t = 5$, $S = 2$, $\sigma_0 = 1 \times 10^{-2}$, and trained DMSTF for 200 epochs on the entire dataset (Full), and also datasets from 9 sites (with more balanced datasets) separately: Caltec, Leuven, MaxMun, NYU, SBL, Stanford, UM, USM, Yale. As shown in Fig. 3 (c) DMSTF and DMSTF+SVM outperform ROI+SVM in Caltec, MaxMun, SBL, Stanford, and Yale, while ROI+SVM only performs better in NYU dataset. DMSTF+SVM performs slightly better than ROI+SVM on the entire dataset (Please note that DMSTF is a clustering approach, hence, no error bars are provided in Fig. 3 (c)). Clustering results for Caltec, Maxmun, SBL, and Stanford are shown in Fig. 3 (a) in which ASD, and control seems to be partially separable (see Fig. S1 in Appendix B for more visualization results).

Depression Dataset: In this dataset [23], 19 individuals with major depressive disorder (MDD) and 20 never-depressed (ND) control participants listened to standardized positive and negative emotional musical and nonmusical stimuli during fMRI scanning. Each participant underwent 3 musical, and 2 nonmusical runs each for 105 time points at TR=3 with $D = 353,600$ voxels. During each run, each stimulus type (positive, and negative) was presented for 33 seconds

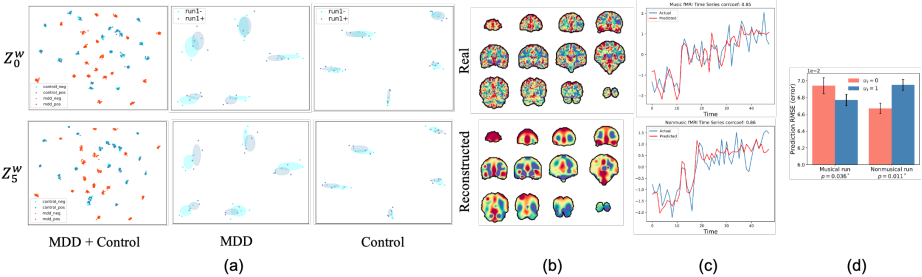


Fig. 4. (a), **Left:** Training DMSTF clustered together temporal latent variables associated with each subject without supervision, while partially separating clusters of points associated with the MDD group from those associated with the control group. The MDD group appears more concentrated into the center of the temporal latent space, while the control group have their temporal latent variables dispersed more broadly across the latent space. (a), **Middle, Right:** DMSTF enabled us to partially separate “positive” and “negative” stimuli per-subject with Gaussian clusters. (b): Real and reconstructed brain images. (c, d): The control variable u_t is a good predictor of temporal sequences in the trained model, with $u_t = 0$ fitting nonmusical sequences and $u_t = 1$ fitting musical sequences. Example fMRI time-series from both musical and nonmusical trials are shown in (c).

(~ 11 time points) interleaved with instances of neutral tone of the same length. We discard instances of neutral tone, and split each run into non-overlapping sequences of $T = 6$ time points in agreement with stimuli design (each stimuli block is split into two sequences). In other words, each run has 4 sequences associated with “positive stimuli”, and 4 with “negative stimuli” resulting in a total of 8 data points for each run. In the **first experiment**, we trained DMSTF on the entire musical runs ($N = 39 \times 3 \times 8 = 936$) by setting $T = 6$, $K = 100$, $D_e = 15$, $D_t = 5$, $\sigma_0 = 1 \times 10^{-3}$ for 200 epochs. The results are shown in Fig. 4 (a, Left). We observed that DMSTF fully separated data points associated with each subject into distinct clusters across the low-dimensional temporal latent space. In other words, DMSTF was able to re-unite pieces of signals associated with each subject without any kind of supervision. More importantly, DMSTF was able to partially separate data points associated with MDD group from control. As seen in Fig. 4 (a, Left), MDD group data points are fairly populated in the center of temporal latent while control group are dispersed across latent space. However, DMSTF was not able to meaningfully separate “negative” and “positive” music pieces in latent embedding from a subject-level perspective, since the variation between runs of a subject dominates stimulus-level variation. For this reason, in a **second experiment**, we focused on 5 subjects, and their first musical run from both MDD and control group and trained DMSTF respectively. Again, as expected, data points from each subject were distinctly clustered in latent space (see middle and right columns in Fig. 4 (a)). Additionally, DMSTF was able to fit two partially separating Gaussians to “positive”, and “negative” stimuli per subject. However, since the number of data points for each subject and run is

Table 2. Held-out Log-Likelihood. DMSTF results in models with higher held-out likelihood, and therefore better fit comparing to HTFA.

Dataset	HTFA	DMSTF
Autism (Caltech)	-2.82×10^6	-2.33×10^6
Depression	-6.64×10^5	-5.71×10^5

limited it is not clear how significant these clusters are. A dataset with longer runs could possibly answer that. In a **third experiment**, we incorporate control inputs u_t , and evaluate prediction performance of DMSTF. We train DMSTF on 2 musical and 1 nonmusical runs for a subject with depression ($8 \times 3 = 24$ sequences) using $u_t = 1$, and $u_t = 0$ respectively (i.e., u_t is encoding musical, nonmusical stimuli). We predict the remaining musical and nonmusical runs ($8 \times 2 = 16$ sequences) once with $u_t = 0$, and another time with $u_t = 1$. As reported in Fig. 4 (d), nonmusical sequences are better predictable with $u_t = 0$ than $u_t = 1$ with $p\text{-value} = 0.011$ (vice versa for musical sequences with $p\text{-value} = 0.036$). Sample predicted fMRI time series from both musical, and nonmusical runs are shown in Fig. 4 (c) (see Fig. S2 in Appendix B for more visualization results).

Comparison with HTFA [24]: We further evaluated DMSTF against HTFA, an established probabilistic model for multi-subject fMRI analysis, which uses unimodal Gaussian priors for both temporal weights, and spatial factor parameters, in terms of held-out log-likelihood (see Table 2). For autism, we used Caltec site dataset, and split each subject’s fMRI into two half (each $T = 70$). We trained DMSTF on the first half, and test on the second half. For depression, we consider 4 sequences from each subject’s run for training, and test on the remaining 4 sequences. To this end, after training DMSTF on each training set, we fixed all parameters of the generative model and only tuned variational parameters of the test set for temporal latents z_t^w, w_t . And finally computed an importance sampling-based estimate of the log-likelihood [22]. The results are shown in Table 2, which proves that DMSTF results in models with higher likelihood on test set, hence a better fit as compared to HTFA.

5.4 Traffic Datasets

Birmingham Dataset ⁵: This dataset recorded occupancy of 30 car parks in Birmingham, UK, from October 4 to December 19, 2016 (77 days) every half an hour between 8 a.m. and 5 p.m. (18 time intervals per day) with 14.89% missing values (completely missing on four days, October 20/21 and December 6/7). We organized the dataset into a tensor of $77 \times 18 \times 30$.

⁵ <https://archive.ics.uci.edu/ml/datasets/Parking+Birmingham>

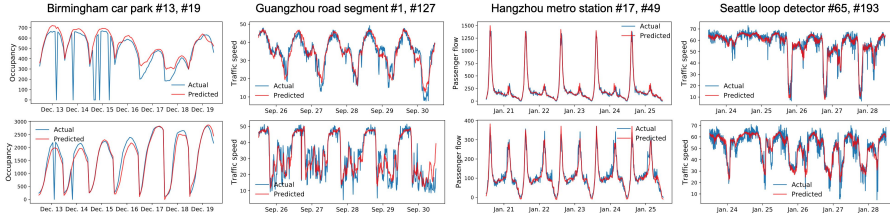


Fig. 5. Predicted time-series for two sample locations in the test-set of each traffic data. Note that the Birmingham and Guangzhou datasets are missing some values, which prediction fills in.

Guangzhou Dataset⁶: This dataset recorded traffic speed data from 214 road segments in Guangzhou, China, from August 1 to September 30, 2016 (61 days) with a 10-minute resolution (144 time intervals per day) with 1.29% missing values. We organized the dataset into a tensor of $61 \times 144 \times 214$.

Hangzhou Dataset⁷: This dataset recorded incoming passenger flow from 80 metro stations in Hangzhou, China, from January 1 to January 25, 2019 (25 days) with a 10-minute resolution during service hours (108 time intervals per day). We organized the dataset into a tensor of $25 \times 108 \times 80$.

Seattle Dataset⁸: This dataset recorded traffic speed from 323 loop detectors in Seattle, USA, over the year of 2015 with a 5-minute resolution (288 time intervals per day). We picked the data from January 1 to January 28 (28 days) as in [8], and organized it into a tensor of $28 \times 288 \times 323$.

Table 3. Performance comparison of short-time prediction. DMSTF outperforms on all datasets, doing significantly better particularly on the Birmingham dataset.

Dataset	Model	DMSTF		BTMF		BayesTRMF		TRMF	
		RMSE	MAPE(%)	RMSE	MAPE(%)	RMSE	MAPE(%)	RMSE	MAPE(%)
Birmingham		102.00	20.24	155.32	25.10	161.11	31.80	174.25	32.63
Guangzhou		4.06	10.19	4.09	10.25	4.27	10.70	4.30	10.65
Hangzhou		34.95	29.87	37.29	30.04	40.87	30.17	39.99	27.77
Seattle		4.49	7.39	4.54	7.48	4.78	7.90	4.90	7.96

We compared DMSTF (variant (a)) with three state-of-the-art baselines on our short-time prediction task: TRMF [44], BayesTRMF developed in [8], and

⁶ <https://doi.org/10.5281/zenodo.1205229>

⁷ <https://tianchi.aliyun.com/competition/entrance/231708/>

⁸ <https://github.com/zhiyongc/Seattle-Loop-Data>

BTMF [8]. We picked the last seven days from the Birmingham dataset, and the last five days from the Guangzhou, Hangzhou, and Seattle datasets for prediction, then trained the models on the rest for each dataset with $K=10, 30, 10, 30$ respectively (consistent setup with [8]). For DMSTF, we additionally set $\{D_z, D_t, D_e\} = 5$, $\sigma_0 = 0$ for all datasets, and learned spatial factors without any functional form constraints. We trained DMSTF for 500 epochs. We report root mean squared error (RMSE), and mean absolute percentage error (MAPE) for all models on the testsets in Table 3. DMSTF outperforms in short-time prediction on all datasets, doing significantly better particularly on the Birmingham dataset. Testset predictions for two sample locations from each dataset are shown in Fig. 5 (see Fig. S3 in Appendix B for a number of long-term prediction visualizations).

6 Conclusion and Future Work

We presented deep Markov spatio-temporal factorization, a new probabilistic model for robust factor analysis of high-dimensional spatio-temporal data. We employed a chain of low-dimensional Markovian latent variables connected by deep neural networks as a state-space embedding for temporal factors in order to model nonlinear dynamics in data, account better for noise and uncertainty, and enable generative prediction. We also employed a low-dimensional spatial embedding to generate a multi-modal distribution of spatial factors. We then demonstrated the tractability of DMSTF on fMRI data (with very high spatial dimensionality) by incorporating functional form assumptions, and on traffic data with high temporal dimensionality. DMSTF enables clustering in the low-dimensional temporal latent space to reveal structure in data (e.g., cognitive states in fMRI), providing informative visualizations about the data. We plan to extend DMSTF to accommodate higher order dynamics for long-term prediction tasks. We can readily achieve this in our setting by conditioning temporal latents on a time-lag set, such as conditioning z_t^w on z_{t-1}^w, z_{t-2}^w in a 2-Markov chain.

References

1. Abraham, A., Milham, M.P., Di Martino, A., Craddock, R.C., Samaras, D., Thirion, B., Varoquaux, G.: Deriving reproducible biomarkers from multi-site resting-state data: An autism-based example. *NeuroImage* **147**, 736–745 (2017)
2. Bahaduri, M.T., Yu, Q.R., Liu, Y.: Fast multivariate spatio-temporal analysis via low rank tensor learning. In: Advances in neural information processing systems. pp. 3491–3499 (2014)
3. Becker, P., Pandya, H., Gebhardt, G., Zhao, C., Taylor, J., Neumann, G.: Recurrent kalman networks: factorized inference in high-dimensional deep feature spaces. arXiv preprint arXiv:1905.07357 (2019)
4. Bonilla, E.V., Chai, K.M., Williams, C.: Multi-task gaussian process prediction. In: Advances in neural information processing systems. pp. 153–160 (2008)
5. Bowman, S.R., Vilnis, L., Vinyals, O., Dai, A.M., Jozefowicz, R., Bengio, S.: Generating sentences from a continuous space. arXiv preprint arXiv:1511.06349 (2015)

6. Cai, Y., Tong, H., Fan, W., Ji, P., He, Q.: Facets: Fast comprehensive mining of coevolving high-order time series. In: Proceedings of the 21th ACM SIGKDD International Conference on Knowledge Discovery and Data Mining. pp. 79–88 (2015)
7. Charlin, L., Ranganath, R., McInerney, J., Blei, D.M.: Dynamic poisson factorization. In: Proceedings of the 9th ACM Conference on Recommender Systems. pp. 155–162 (2015)
8. Chen, X., He, Z., Chen, Y., Lu, Y., Wang, J.: Missing traffic data imputation and pattern discovery with a bayesian augmented tensor factorization model. Transportation Research Part C: Emerging Technologies **104**, 66–77 (2019)
9. Chen, Z., Cichocki, A.: Nonnegative matrix factorization with temporal smoothness and/or spatial decorrelation constraints. Laboratory for Advanced Brain Signal Processing, RIKEN, Tech. Rep **68** (2005)
10. Cichocki, A.: Tensor decompositions: a new concept in brain data analysis? arXiv preprint arXiv:1305.0395 (2013)
11. Comon, P., Jutten, C., Herault, J.: Blind separation of sources, part ii: Problems statement. Signal processing **24**(1), 11–20 (1991)
12. Craddock, C., Benhajali, Y., Chu, C., Chouinard, F., Evans, A., Jakab, A., Khundrakpam, B.S., Lewis, J.D., Li, Q., Milham, M., et al.: The neuro bureau preprocessing initiative: open sharing of preprocessed neuroimaging data and derivatives. Frontiers in Neuroinformatics **7** (2013)
13. Fraccaro, M., Kamronn, S., Paquet, U., Winther, O.: A disentangled recognition and nonlinear dynamics model for unsupervised learning. In: Advances in Neural Information Processing Systems. pp. 3601–3610 (2017)
14. Hoffman, M.D., Blei, D.M., Wang, C., Paisley, J.: Stochastic variational inference. The Journal of Machine Learning Research **14**(1), 1303–1347 (2013)
15. Hopkins, S.B., Shi, J., Steurer, D.: Tensor principal component analysis via sum-of-square proofs. In: Conference on Learning Theory. pp. 956–1006 (2015)
16. Jiang, Z., Zheng, Y., Tan, H., Tang, B., Zhou, H.: Variational deep embedding: An unsupervised and generative approach to clustering. arXiv preprint arXiv:1611.05148 (2016)
17. Jing, P., Su, Y., Jin, X., Zhang, C.: High-order temporal correlation model learning for time-series prediction. IEEE transactions on cybernetics **49**(6), 2385–2397 (2018)
18. Karl, M., Soelch, M., Bayer, J., van der Smagt, P.: Deep variational bayes filters: Unsupervised learning of state space models from raw data. arXiv preprint arXiv:1605.06432 (2016)
19. Kingma, D.P., Ba, J.: Adam: A method for stochastic optimization. arXiv preprint arXiv:1412.6980 (2014)
20. Kingma, D.P., Welling, M.: Auto-encoding variational bayes. arXiv preprint arXiv:1312.6114 (2013)
21. Krishnan, R.G., Shalit, U., Sontag, D.: Deep kalman filters (2015)
22. Krishnan, R.G., Shalit, U., Sontag, D.: Structured inference networks for nonlinear state space models. In: Thirty-First AAAI Conference on Artificial Intelligence (2017)
23. Lepping, R.J., Atchley, R.A., Chrysikou, E., Martin, L.E., Clair, A.A., Ingram, R.E., Simmons, W.K., Savage, C.R.: Neural processing of emotional musical and nonmusical stimuli in depression. PloS one **11**(6), e0156859 (2016)
24. Manning, J.R., Ranganath, R., Keung, W., Turk-Browne, N.B., Cohen, J.D., Norman, K.A., Blei, D.M.: Hierarchical topographic factor analysis. In: 2014 International Workshop on Pattern Recognition in Neuroimaging. pp. 1–4. IEEE (2014)

25. Manning, J.R., Ranganath, R., Norman, K.A., Blei, D.M.: Topographic factor analysis: a bayesian model for inferring brain networks from neural data. *PloS one* **9**(5), e94914 (2014)
26. Melkumyan, A., Ramos, F.: Multi-kernel gaussian processes. In: Twenty-second international joint conference on artificial intelligence (2011)
27. Parisot, S., Ktena, S.I., Ferrante, E., Lee, M., Moreno, R.G., Glocker, B., Rueckert, D.: Spectral graph convolutions for population-based disease prediction. In: International conference on medical image computing and computer-assisted intervention. pp. 177–185. Springer (2017)
28. Paszke, A., Gross, S., Chintala, S., Chanan, G., Yang, E., DeVito, Z., Lin, Z., Desmaison, A., Antiga, L., Lerer, A.: Automatic differentiation in pytorch (2017)
29. Pearson, K.: Liii. on lines and planes of closest fit to systems of points in space. *The London, Edinburgh, and Dublin Philosophical Magazine and Journal of Science* **2**(11), 559–572 (1901)
30. Ranganath, R., Wang, C., David, B., Xing, E.: An adaptive learning rate for stochastic variational inference. In: International Conference on Machine Learning. pp. 298–306 (2013)
31. Rezende, D.J., Mohamed, S.: Variational inference with normalizing flows. arXiv preprint arXiv:1505.05770 (2015)
32. Richard, E., Montanari, A.: A statistical model for tensor pca. In: Advances in Neural Information Processing Systems. pp. 2897–2905 (2014)
33. Rogers, M., Li, L., Russell, S.J.: Multilinear dynamical systems for tensor time series. In: Advances in Neural Information Processing Systems. pp. 2634–2642 (2013)
34. Salakhutdinov, R., Mnih, A.: Bayesian probabilistic matrix factorization using markov chain monte carlo. In: Proceedings of the 25th international conference on Machine learning. pp. 880–887 (2008)
35. Sennesh, E., Khan, Z., Dy, J., Satpute, A.B., Hutchinson, J.B., van de Meent, J.W.: Neural topographic factor analysis for fmri data (2019)
36. Singh, C., Wang, B., Qi, Y.: A constrained, weighted-l1 minimization approach for joint discovery of heterogeneous neural connectivity graphs. arXiv preprint arXiv:1709.04090 (2017)
37. Sun, J.Z., Parthasarathy, D., Varshney, K.R.: Collaborative kalman filtering for dynamic matrix factorization. *IEEE Transactions on Signal Processing* **62**(14), 3499–3509 (2014)
38. Sun, L., Chen, X.: Bayesian temporal factorization for multidimensional time series prediction. arXiv preprint arXiv:1910.06366 (2019)
39. Takeuchi, K., Kashima, H., Ueda, N.: Autoregressive tensor factorization for spatio-temporal predictions. In: 2017 IEEE International Conference on Data Mining (ICDM). pp. 1105–1110. IEEE (2017)
40. Tzourio-Mazoyer, N., Landeau, B., Papathanassiou, D., Crivello, F., Etard, O., Delcroix, N., Mazoyer, B., Joliot, M.: Automated anatomical labeling of activations in spm using a macroscopic anatomical parcellation of the mni mri single-subject brain. *Neuroimage* **15**(1), 273–289 (2002)
41. Vasilescu, M.A.O., Terzopoulos, D.: Multilinear independent components analysis. In: 2005 IEEE Computer Society Conference on Computer Vision and Pattern Recognition (CVPR'05). vol. 1, pp. 547–553. IEEE (2005)
42. Watter, M., Springenberg, J., Boedecker, J., Riedmiller, M.: Embed to control: A locally linear latent dynamics model for control from raw images. In: Advances in neural information processing systems. pp. 2746–2754 (2015)

43. Xiong, L., Chen, X., Huang, T.K., Schneider, J., Carbonell, J.G.: Temporal collaborative filtering with bayesian probabilistic tensor factorization. In: Proceedings of the 2010 SIAM international conference on data mining. pp. 211–222. SIAM (2010)
44. Yu, H.F., Rao, N., Dhillon, I.S.: Temporal regularized matrix factorization for high-dimensional time series prediction. In: Advances in neural information processing systems. pp. 847–855 (2016)
45. Zhao, Q., Zhang, L., Cichocki, A.: Bayesian cp factorization of incomplete tensors with automatic rank determination. IEEE transactions on pattern analysis and machine intelligence **37**(9), 1751–1763 (2015)

A Derivation of Evidence Lower BOund (ELBO) for DMSTF

We derive the lower bound on the log-likelihood of observations by incorporating conditional independences inferred from the graphical model of DMSTF in Fig. 1 (c) as follows:

$$Y_n \perp\!\!\!\perp Y_{\neg n} | w_{n,1:T}, H_n , \quad z_{n,t}^w \perp\!\!\!\perp z_{n,\neg(t,t-1)}^w | z_{n,t-1}^w , \quad z_{n,t}^w \perp\!\!\!\perp z_{\neg n}^w | z_{n,t-1}^w \\ z_{n,0}^w \perp\!\!\!\perp z_{\neg n,0}^w | c_n , \quad w_{n,t} \perp\!\!\!\perp w_{n,\neg t} | z_{n,t}^w , \quad w_{n,t} \perp\!\!\!\perp w_{\neg n} | z_{n,t}^w , \quad H_n \perp\!\!\!\perp H_{\neg n} | z_n^f$$

Considering these conditional independencies, the joint distribution of observations and latent variables will be (denoting $Z = \{z^w, z^f\}$):

$$p_\theta(Y, c, Z, W, H|u) = \prod_{n=1}^N p_\theta(Y_n|w_{n,1:T}, H_n) p_\theta(H_n|z_n^f) p_\theta(z_n^f) p_\theta(z_{n,0}^w|c_n) p_\theta(c_n) \\ \prod_{t=1}^T p_\theta(w_{n,t}|z_{n,t}^w) p_\theta(z_{n,t}|z_{n,t-1}, u_{n,t-1}) \quad (1)$$

We assume a fully factorized variational distribution on $\{c, z^f, z_0^w, w\}$, and a structured variational distribution on $q_\phi(z_{1:T}^w|w_{1:T})$, hence:

$$q_\phi(c, Z, W, H|Y, u) = \prod_{n=1}^N q_\phi(c_n) q_\phi(z_n^f) q_\phi(H_n) q_\phi(z_{n,0}^w) \\ \prod_{t=1}^T q_\phi(z_{n,t}^w|z_{n,t-1}^w, w_{n,1:T}) q_\phi(w_{n,t}) \quad (2)$$

We then derive the ELBO by writing down the log-likelihood of observations, and plugging in $p(\cdot)$ and $q(\cdot)$ from Equation (1) and Equation (2) respectively (we denote continuous latent variables collectively as $\mathcal{Z} = \{Z, W, H\}$ for brevity):

$$\log p_\theta(Y|u) = \log \sum_c \int_{\mathcal{Z}} q_\phi(c, \mathcal{Z}|Y, u) \frac{p_\theta(Y, c, \mathcal{Z}|u)}{q_\phi(c, \mathcal{Z}|Y, u)} d\mathcal{Z} \\ \geq_{\{\text{Jensen's inequality}\}} \sum_c \int_{\mathcal{Z}} q_\phi(c, \mathcal{Z}|Y, u) \log \frac{p_\theta(Y, c, \mathcal{Z}|u)}{q_\phi(c, \mathcal{Z}|Y, u)} d\mathcal{Z}$$

$$\begin{aligned}
&= \sum_c \int_{\mathcal{Z}} q(c, \mathcal{Z} | Y, u) \cdots \\
&\log \prod_{n=1}^N \frac{p(Y_n | w_{n,1:T}, H_n) p(H_n | z_n^f) p(z_n^f) p(z_{n,0}^w | c_n) p(c_n)}{q(H_n) q(z_n^f) q(z_{n,0}^w) q(c_n)} \cdots \\
&\prod_{t=1}^T \frac{p(w_{n,t} | z_{n,t}^w) p(z_{n,t}^w | z_{n,t-1}^w, u_{n,t-1})}{q(w_{n,t}) q(z_{n,t}^w | z_{n,t-1}^w, w_{n,1:T})} d\mathcal{Z} \\
&= \sum_{c \setminus c'} q(c \setminus c') \int_{\mathcal{Z} \setminus z'} q(\mathcal{Z} \setminus z') d\mathcal{Z} \sum_{n=1}^N \cdots \\
&\int_{\substack{z' = \{w_{n,1:T}, H_n\} \\ c' = \emptyset}} q(w_{n,1:T}, H_n) \log p(Y_n | w_{n,1:T}, H_n) dz' + \\
&\sum_{\substack{c' = \{c_n\} \\ z' = \emptyset}} q(c_n) \log \frac{p(c)}{q(c_n)} + \sum_{c' = \{c_n\}} q(c_n) \int_{\substack{z' = \{z_{n,0}^w\}}} q(z_{n,0}^w) \log \frac{p(z_{n,0}^w | c_n)}{q(z_{n,0}^w)} dz' + \\
&\sum_{t=1}^T \int_{\substack{z' = \{w_{n,1:T}, z_{n,t-1}^w, z_{n,t}^w\} \\ c' = \emptyset}} q(w_{n,1:T}) q(z_{n,t-1}^w | w_{n,1:T}) \cdots \\
&q(z_{n,t}^w | z_{n,t-1}^w, w_{n,1:T}) \log \frac{p(z_{n,t}^w | z_{n,t-1}^w, u_{n,t-1})}{q(z_{n,t}^w | z_{n,t-1}^w, w_{n,1:T})} dz' + \\
&\sum_{t=1}^T \int_{\substack{z' = \{z_{n,t}^w, w_{n,t}\} \\ c' = \emptyset}} q(z_{n,t}^w) q(w_{n,t}) \log \frac{p(w_{n,t} | z_{n,t}^w)}{q(w_{n,t})} dz' + \\
&\int_{\substack{z' = \{z_n^f, H_n\} \\ c' = \emptyset}} q(z_n^f) q(H_n) \log \frac{p(H_n | z_n^f)}{q(H_n)} dz' + \int_{\substack{z' = \{z_n^f\} \\ c' = \emptyset}} q(z_n^f) \log \frac{p(z_n^f)}{q(z_n^f)} dz', \quad (3)
\end{aligned}$$

where the integration over distributions of latent variables outside of the summation over n is $\sum_{c \setminus c'} q(c \setminus c') \int_{\mathcal{Z} \setminus z'} q(\mathcal{Z} \setminus z') d\mathcal{Z} \setminus z' = 1$ for $\{c', z'\}$ of each term inside the summation (we are abusing notation here, for the sake of brevity). Considering that $\text{KL}(q, p) = \int q \log \frac{q}{p}$, and $\mathbb{E}_{q(x)}[f(x)] = \int_x q(x) f(x)$, we can rewrite each term of the summation in Equation (3) to summarize the ELBO:

$$\log p_\theta(Y | u) \geq \sum_{n=1}^N \left(\mathcal{L}_n^{\text{rec}} + \mathcal{L}_n^C + \sum_{t=1}^T (\mathcal{L}_{t,n}^{z^w} + \mathcal{L}_{t,n}^W) + \mathcal{L}_n^H \right), \quad (4)$$

where,

$$\begin{aligned}\mathcal{L}_n^{\text{rec}} &= \mathbb{E}_{q_\phi(w_{n,1:T}, H_n)} [\log p_\theta(Y_n | w_{n,1:T}, H_n)] \\ \mathcal{L}_n^C &= -\mathbb{KL}(q_\phi(c_n) || p_\theta(c)) - \sum_{c_n} q_\phi(c_n) \mathbb{KL}(q_\phi(z_{n,0}^w) || p_\theta(z_{n,0}^w | c_n)) \\ \mathcal{L}_{n,t}^w &= -\mathbb{E}_{q_\phi(w_{n,1:T})} \mathbb{E}_{q_\phi(z_{n,t-1}^w | w_{n,1:T})} [\mathbb{KL}(q_\phi(z_{n,t}^w | z_{n,t-1}^w, w_{n,1:T}) || p_\theta(z_{n,t}^w | z_{n,t-1}^w, u_{n,t-1}))] \\ \mathcal{L}_{n,t}^W &= -\mathbb{E}_{q_\phi(z_{n,t}^w)} [\mathbb{KL}(q_\phi(w_{n,t}) || p_\theta(w_{n,t} | z_{n,t}^w))] \\ \mathcal{L}_{n,t}^H &= -\mathbb{E}_{q_\phi(z_n^f)} [\mathbb{KL}(q_\phi(H_n) || p_\theta(H_n | z_n^f)) - \mathbb{KL}(q_\phi(z_n^f) || p_\theta(z^f))].\end{aligned}$$

Kulback Leibler (KL) Divergence Terms: We can analytically calculate the KL terms of ELBO in Equation (4). For two multivariate (d -dimensional) Gaussian distributions $q(\cdot)$, and $p(\cdot)$, the KL divergence is:

$$\mathbb{KL}(q, p) = \frac{1}{2} \left[\log \frac{|\Sigma_p|}{|\Sigma_q|} - d + \text{tr}(\Sigma_p^{-1} \Sigma_q) + (\mu_p - \mu_q)^T \Sigma_p^{-1} (\mu_p - \mu_q) \right],$$

which would be further simplified here, in the case of diagonal covariances. The KL divergence between two S -dimensional categorical distributions $q(\cdot)$ and $p(\cdot)$ can be readily computed:

$$\mathbb{KL}(q, p) = \sum_s q_s \log \left(\frac{q_s}{p_s} \right),$$

where the subscript s denotes the probability of state s out of S possible states.

B More Visualizations for Autism, Depression, and Traffic Datasets

We have visualized real and reconstructed brain images from the nine subsets of autism dataset (Caltex, Leuven, MaxMun, NYU, SBL, Stanford, UM, USM, and Yale sites) along with z_0^w after training DMSTF on the full autism dataset in Fig. S1. DMSTF clustered together temporal latent variables associated with each acquisition site without supervision in z_0^w . As depicted, the variation among different acquisition sites dominates the cognitive differences between ASD group and control, hence, a downstream connectivity matrix classification (using learned temporal weights, W) helps better in differentiating ASD group from control in multi-site analysis.

In Fig. S2, we have visualized example predicted fMRI time-series from both musical and non-musical trials in the test-set of depression dataset using control variable $u_t = 1$ for musical and $u_t = 0$ for non-musical trials.

In Fig. S3, we have visualized next-day (long-term) prediction results for Birmingham and Huangzhou subsets of traffic data for four sample locations. These predictions are purely obtained from the trained temporal generative model. Please note that the actual values for the predicted days are not available.

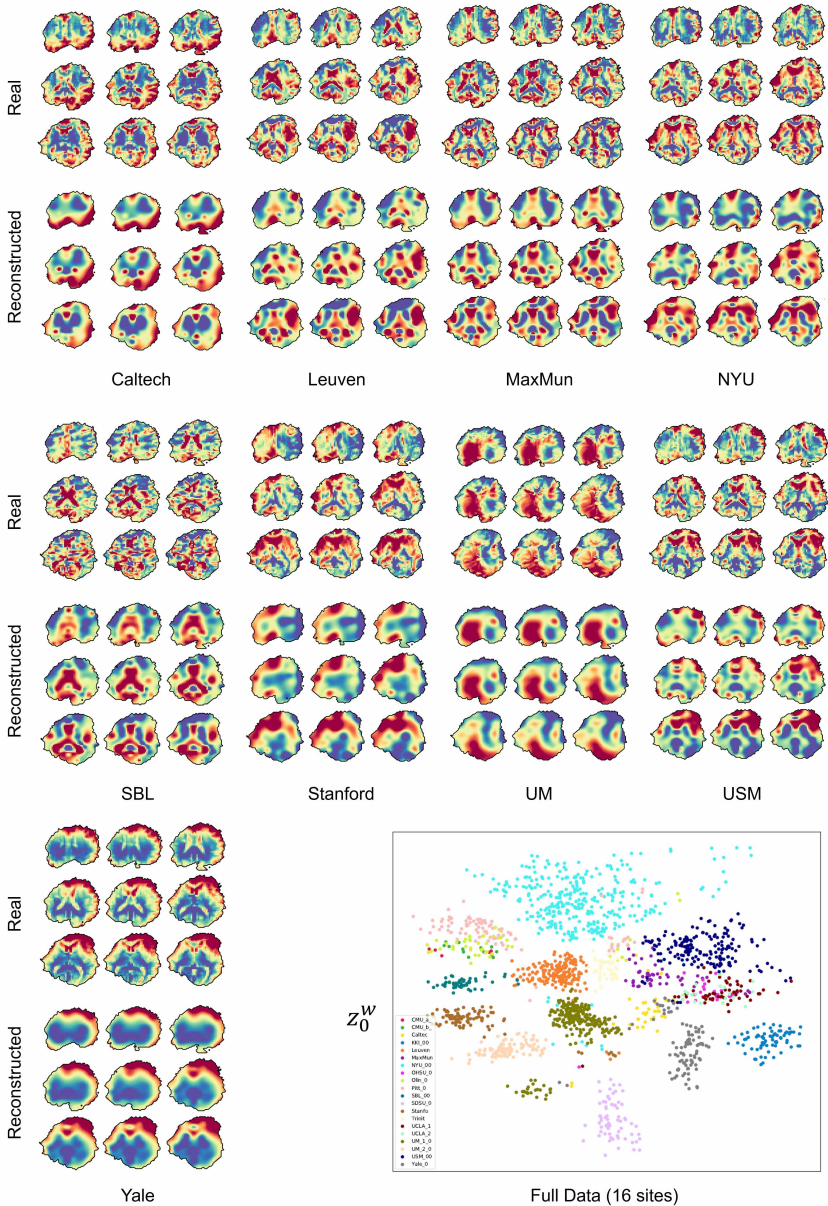


Fig. S1. Real and reconstructed brain images from the nine subsets of Autism dataset (Caltech, Leuven, MaxMun, NYU, SBL, Stanford, UM, USM, and Yale sites) showing the smoothing given by sparse factorization. **Visualizing** z_0^W after training DMSTF on the full autism dataset. DMSTF clustered together temporal latent variables associated with each acquisition site without supervision. As depicted, the variation among different acquisition sites dominates the variation in cognitive state of the brain (ASD group vs. control), hence, a downstream connectivity matrix classification helps better in differentiating ASD group from control in multi-site analysis.

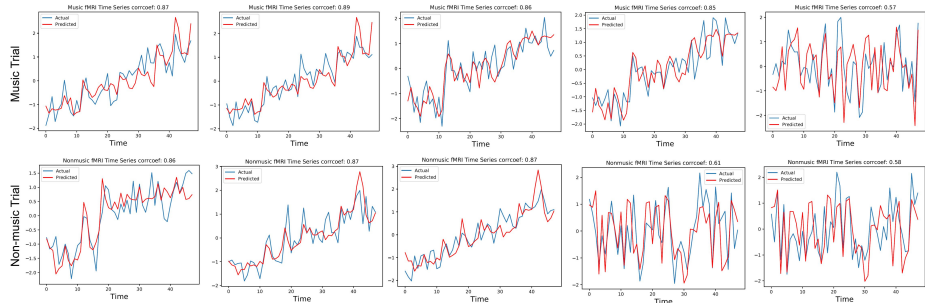


Fig. S2. Example fMRI time-series from both musical and non-musical trials (in the test-set of depression dataset) predicted with control variable $u_t = 1$ for musical and $u_t = 0$ for non-musical trials.

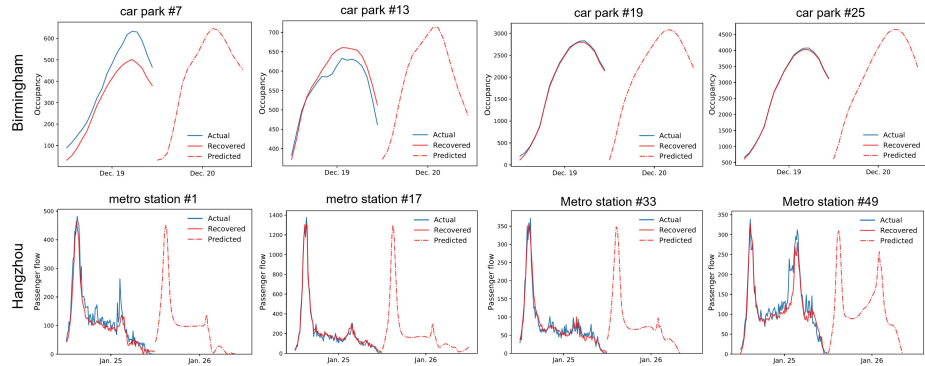


Fig. S3. Visualizing next-day (long-term) prediction results for Birmingham and Huangzhou subsets of traffic data for four sample locations. Although DMSTF is well-suited for short-time prediction, next-day forecasts (purely from the trained temporal generative model) show its capability in long-term predictions. Please note that the actual values for the predicted days are not available.